Materials Science and Engineering A 545 (2012) 225–228

Contents lists available at SciVerse ScienceDirect

Materials Science and Engineering A

journal homepage: www.elsevier.com/locate/msea

Rapid communication

Further evidence for room temperature, indentation-induced nanocrystallization in a bulk metallic glass

Byung-Gil Yoo[a], In-Chul Choi[a], Yong-Jae Kim[a], Jin-Yoo Suh[b], Upadrasta Ramamurty[c], Jae-il Jang[a,*]

[a] Division of Materials Science and Engineering, Hanyang University, Seoul 133-791, Republic of Korea
[b] High Temperature Energy Materials Center, Korea Institute of Science and Technology, Seoul 136-791, Republic of Korea
[c] Department of Materials Engineering, Indian Institute of Science, Bangalore 560012, India

ARTICLE INFO

Article history:
Received 9 December 2011
Received in revised form 8 February 2012
Accepted 8 March 2012
Available online 21 March 2012

Keywords:
Bulk metallic glass
Nanoindentation
Nanocrsytallization

ABSTRACT

Room temperature nanoindentation experiments, employing two different pyramidal (Berkovich and cube-corner) indenters, were performed on a Zr-based bulk metallic glass (BMG) to critically examine the possibility of indentation-induced nanocrystallization in BMGs. Cross-sectional transmission electron microscopy images obtained from high angle annular dark field (HAADF) and high resolution (HR) modes clearly indicate to the occurrence of nanocrystallization. Pronounced nanocrystallite formation in the case of sharper cube-corner indenter suggests that the structural transformation is favored by the high strains introduced during nanoindentation.

1. Introduction

Recently, many research efforts have been made for a better understanding of the mechanical behavior of bulk metallic glasses (BMGs) so as to improve their mechanical properties (especially plasticity) and in turn make them more suitable materials for structural and engineering applications [1]. Since BMGs are metastable in nature, it is likely that severe plastic deformation could impart certain structural changes, which include the possibility of deformation-induced nanocrystallization. This possibility has an importance from both scientific and engineering viewpoints as such chemical heterogeneities in amorphous matrix are often thought to conceivably play a role in enhancing the plasticity and toughness of the material [1,2]. Early work of Chen et al. [3] and later by Jiang and Atzmon [4] demonstrated nanocrystallization in/near the shear bands on Al-based rapidly quenched amorphous ribbon. However, it is noteworthy that the amorphous alloys used in these studies are only 'marginal glasses' having relatively low glass forming ability and hence are highly metastable, i.e. susceptible readily to deformation-induced nanocrystallization.

In contrast, BMGs are made of alloys which are excellent glass formers and hence are more stable. Through transmission electron microscopy (TEM) analysis, Kim et al. [5] reported indentation-induced crystallization in a Zr-based BMG with nanocrystallites of 10–40 nm in diameter that was subjected to quasi-static sharp indentation (with a Berkovich tip) at room temperature. By way of a mechanistic rationalization, they argue that the local dilatation in shear bands increases diffusivity, which in turn facilitates nanocrystal formation. Schuh and Nieh [6], on the other hand, did not observe any indentation-induced crystallization but only indications of clusters of medium range order (MRO), whose size is about 2 nm. Kramer et al. [7] studied the deformation zone formed by cylindrical indenter using high energy synchrotron X-ray diffraction (XRD) as well as TEM and reported no evidence of indentation-induced crystallization. More recently, Fornell et al. [8] reported the indentation-induced nanocrystallization in a Zr–Cu–Ni–Al BMG through in-plane TEM analysis. Due to this inconsistency in the reported data regarding the indentation-induced nanocrystallization, the possibility of it being an artifact of the experimental techniques employed has come into question. This dispute is mainly based on the fact that Kim et al. [5] and Fornell et al. [8] did not use the cross-sectional TEM images but the in-plane TEM images of mechanically thinned and ion-milled samples, which do not rule the possibility of nanocrystallization taking place during TEM sample preparation out. There are two possible ways for this to occur: first, extensive deformation during mechanical thinning or dimpling and second, microstructural changes during ion-milling either due to ion bombardment or due to sample heating. An additional, and important, point is the following. In Refs. [5,8], in-plane TEM analysis was utilized, which makes it difficult to precisely identify the area of interest with respect to the indenter tip. Typically, indentation with a sharp tip results in a large gradients in the stress and strain fields underneath the indenter [9]. Thus, the inability to locate the field view precisely with the

* Corresponding author. Fax: +82 2 2220 0389.
E-mail address: jijang@hanyang.ac.kr (J.-i. Jang).

0921-5093/$ – see front matter © 2012 Elsevier B.V. All rights reserved.
doi:10.1016/j.msea.2012.03.026

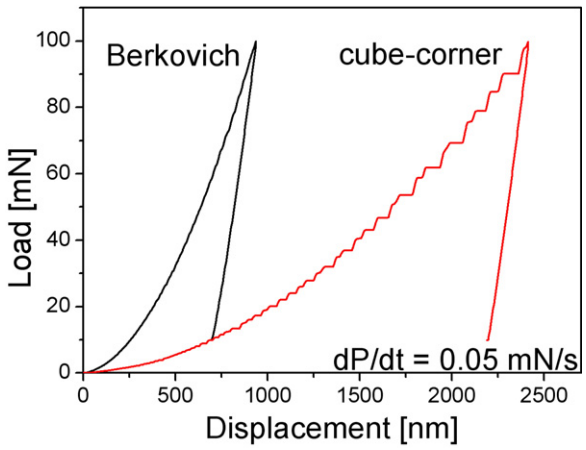

Fig. 1. Nanoindentation load–displacement curves made with cube-corner and Berkovich indenters to a peak load P_{max} = 100 mN and loading rate dP/dt = 0.05 mN/s.

indenter tip precludes the possibility of correlating the indentation strain fields with nanocrystallization levels.

The above brief summary clearly suggests that the literature is not in unison and whether or not crystallization occurs during nanoindentation at room temperature. Hence the question, 'is the reported crystallization a fact or an artifact?' is yet to be answered. The purpose of this paper is to report experimental results that further provide an evidence for the nanocrystallization during room temperature indentation of a BMG.

2. Experimental

The BMG examined in this study is a Zr-based BMG, $Zr_{52.5}Cu_{17.9}Ni_{14.6}Al_{10}Ti_5$ (often referred to as Vit 105) that is known to have an excellent glass forming ability. The composition of this alloy is the same as that in Kim et al.'s work [5] where the indentation-induced nanocrystallization was reported. Disk-shaped specimens were cut from a BMG rod having diameter and length of about 7 and 70 mm, respectively, and then mechanically polished. The amorphous nature of the sample was confirmed by the absence of crystalline peak in the XRD scan (shown elsewhere [10]). Nanoindentations were made on a mirror-finished sample using the Nanoindenter-XP (Agilent Corp., Oak Ridge, TN, USA) with two triangular pyramid indenters having centerline-to-face angles of 35.3° (cube-corner indenter) and 65.3° (Berkovich indenter). All indentation tests were performed to a peak load of 100 mN at loading/unloading rates of 0.05 mN/s.

Focused Ion Beam (FIB; Nova 200 NanoLab, FEI Co, Hillsboro, OR) was used to prepare cross-sectional TEM (XTEM) specimens. At around the vertex of the indented impression, a thin slice, for which out of plane direction is normal to the specimen surface, is FIB milled and lifted to provide cross-sectional view of the microstructure right underneath the indenter tip. Special care was taken during the FIB milling process so as to minimize the possibility of beam-induced heating. This was done by keeping the Ga ion beam intensity and acceleration voltage as low as 10 pA and 30 kV, respectively. High angle annular dark field (HAADF) imaging under scanning transmission electron microscopy (STEM) and high-resolution (HR) imaging techniques were utilized to investigate the distribution of the nanocrystallites using Tecnai F20 TEM (FEI Co., Hillsboro, OR).

3. Results and discussion

Fig. 1 shows representative nanoindentation load–displacement (P–h) curves where the sharper cube-corner indenter produces a larger depth of penetration at a given load and a greater proportion of permanent plastic deformation after unloading than the Berkovich indenter. Although the P–h curves of Fig. 1 obtained from both indenters do not indicate any indentation-induced crystallization, they confirm the idea that the sharper cube-corner indenter displaces much more volume, thereby produces greater stresses and strains for a given load [11–13]. Additional important feature in the P–h curve obtained with the cube-corner indenter is the occurrence of pronounced 'pop-ins' (that are often associated with the shear-band-mediated plastic flow) vis-à-vis the Berkovich indentation; i.e., the latter shows 'ripples' rather than the 'pop-ins,' which is conceivably due to the high indentation strains induced by the cube-corner indenter. This, in turn, can be expected to cause some 'magnification' in indentation-induced crystallization in BMGs. Additionally, the use of dual indenters may provide an important clue for the source of nanocrystallization, if any; if the formation of nanocrystallites is more pronounced in the cube-corner indentation than in the Berkovich indentation, it is possible to deduce that the nanocrystallization is due to the indentation stresses and strains rather than other causes such as ion beam heating.

Fig. 2 shows XTEM images of the area located right underneath the indent acquired in HAADF mode. Since the contrast here is associated with the average atomic number, resulting in so-called Z-contrast, as well as the local thickness variation of the specimen [14], HAADF image can be used as direct proof of phase separation and nanocrystallization in metallic glasses.

As shown in Fig. 2(a), for the specimen indented by the Berkovich tip, the formation of nanocrystallites is observed. However, they are limited to the boundary area which was in contact with the indenter tip. On the other hand, such a region obtained from cube-corner indentation is more pronounced as shown in Fig. 2(b). A magnified view of the region near the contact is shown in Fig. 2(c), which indicates that the size of the crystallites ranges from 2 to 6 nm. Comparison of Fig. 2(a) and (b) suggests that the area containing crystallites in the cube-corner indentation appears wider.

As seen in the figures, the nanocrystallites were not found all over the specimen, in other words, they were found only underneath the contact with indenter tip. This observation suggests that it is closely related to the stress and strain state produced by the indentation. Although there is always a possibility of nanocrystallization induced by ion bombardments during FIB sample preparation process, the non-uniform distribution of the nanocrystallites observed in the samples excludes such a possibility. In addition, oxidation and Ga ion effects were checked by using energy-dispersive X-ray spectroscopy (EDX or EDS). Although Pt coating layer was deposited near the indent, any Pt-contaminated region around the area close to the indent could not be found. Overall, the possibility of Pt-contamination for the white spots observed underneath the indent was excluded.

To reconfirm the existence of the nanocrystallites, the HRTEM analysis of cube-corner indentation was additionally carried out as shown in Fig. 3. The HR image was taken from approximately the same location as that in Fig. 2(c). Since the size of our available selected aperture area (with a diameter of 180 nm) is too big as compared to the size of the nanocrystallites, we could not obtain selected area electron diffraction (SAED) patterns of them. Instead, small areas exhibiting localized lattice patterns and thus appearing to form crystalline structure (marked by circles and ellipses) were digitally analyzed and the corresponding Fast Fourier transform (FFT) patterns were obtained. The FFT patterns of area A and B in the figure are provided as inset images. Note that FFT also could not provide clear diffraction pattern of the nanocrystallites due to their limited size and number density. The arrows in the insets, showing diffraction spots of nanocrystallites, turned out to

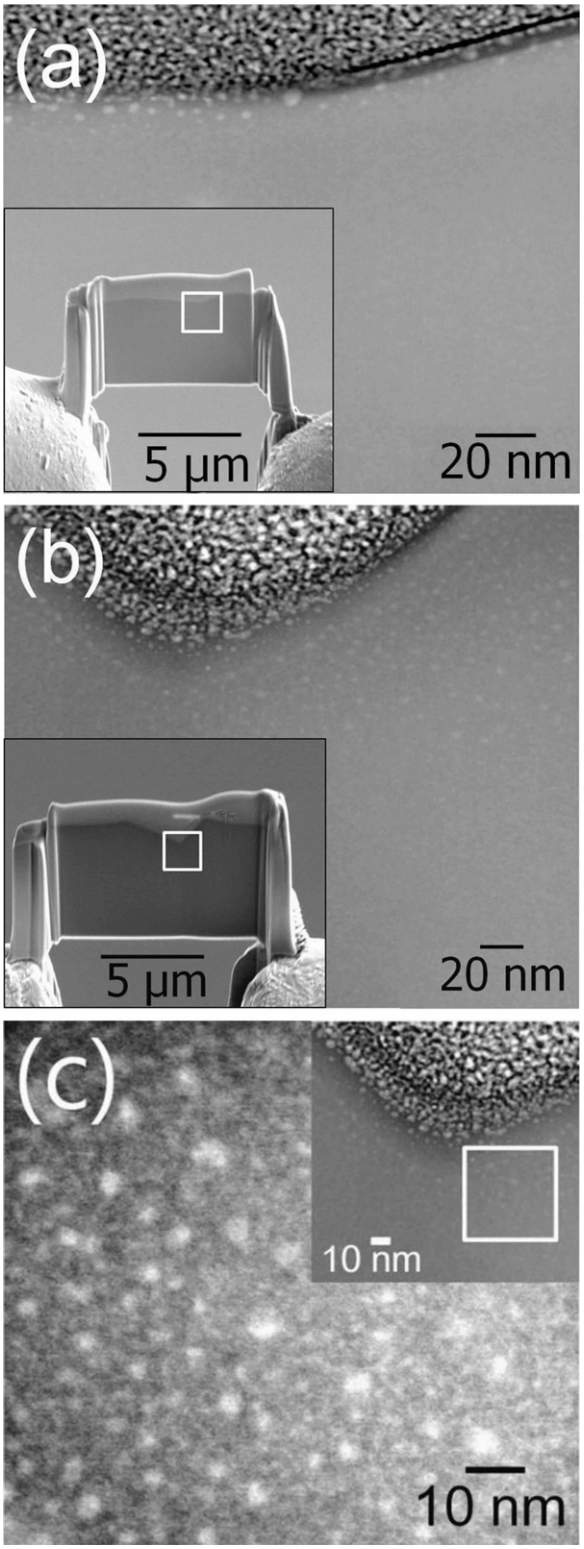

Fig. 2. Images of TEM analysis under HAADF mode: (a) Berkovich and (b) cube-corner indentation. Inset images of (a) and (b) exhibit the locations for the FIB process. A magnified image for the region close to the contact surface in (b) is provided in (c).

originate from the individual crystallites (indicated by the other arrows) inside the squares for the area A and B; the diffraction of nanocrystallites is originated from the lattice planes with 0.216 and 0.188 nm interplanar distances. To remove the possibility of artifact of Pt contamination from sample preparation by

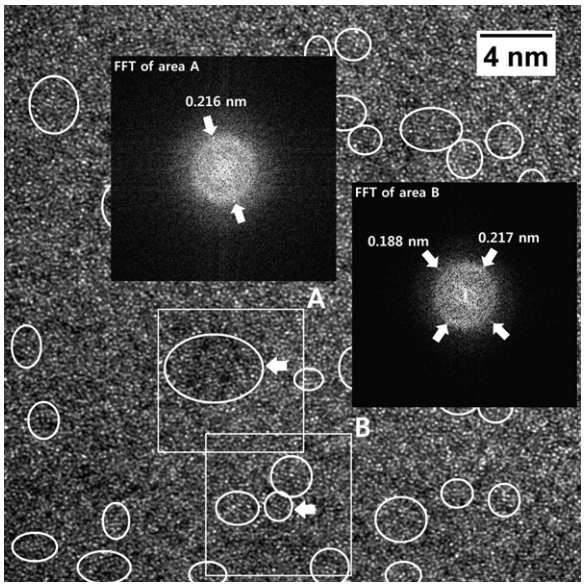

Fig. 3. HRTEM image and FFT patterns for selected areas in the subsurface region underneath the cube-corner indenter.

FIB milling, HR lattice images of Pt crystal taken near the interface area were also analyzed (not shown here) and compared with the results in Fig. 3. The comparison clearly indicated that the nanocrystallites in Fig. 3 are not Pt whose major d-spacings are 0.227, 0.196, and 0.139 for 111, 200, and 220 planes, respectively. Although more evidence is required to identify and confirm the crystal structure of the nanocrystallites, the 0.216 and 0.188 nm d-spacings could be results of 440 and 622 diffractions, respectively, of cubic $NiZr_2$ intermetallic phase with lattice constant of 12.27 Å (space group Fd3m), which was also observed by Altounian et al. [15]. Particularly the crystal located right on center of the squared area B (marked by an arrow) shows two diffractions together, as shown in the second inset, with angle of 77.7° which is close to the angle, 77.1°, between two diffraction spots of 022 and 620 with a zone axis of 133. However, note that the stable form of $NiZr_2$ is tetragonal (space group I4/mcm, a = 6.49 Å, c = 5.28 Å) and Kim et al. [5] indexed a similarly obtained phase as such. Considering that the crystallites size is larger in Ref. [5] (10–40 nm) than in this study (<5 nm), the disagreement in the crystal structure arrived at in this study and that of Kim et al. could be attributed to a possible structural transition from metastable cubic (at early stage) to stable tetragonal upon growth. Or, the disagreement could have origins in the possible difference in the amount of impurities such as oxygen [15]. Further studies are required to clarify this. Overall, the HR image exhibits abundance of nanocrystallites, with sizes less than 5 nm, embedded homogeneously in the amorphous matrix near the contact surface. The size of the nanocrystallites observed by the HR images agrees well with the observation on the 'compositional heterogeneities' made by HAADF mode. It is informative to note that the density of the nanocrystallites in the HR image (Fig. 3) appears lower than that of the HAADF image (Fig. 2(c)). This is possibly due to the fact that only the crystals properly aligned to the electron beam direction would make meaningful phase contrast in HR image, while all of the 'compositional heterogenities' could be detected in STEM-HAADF mode; i.e. not all of the existing nanocrystallites are seen in HR image. Thus, the HRTEM analysis further confirms that nanoindentation-generated deformation certainly promotes nanocrystallization.

4. Conclusions

By adopting two approaches, our experiments unambiguously confirm nanoindentation-induced nanocrystallization in BMGs. First, nanoindentations were performed with two different three-sided pyramidal indenters, which induce different levels of strains underneath. TEM observations revealed that higher strains certainly led to higher amount of nanocrystals, which implies that the crystallization is indeed caused by indentation-induced plastic deformation. Second, a cross-sectional TEM analysis was applied instead of in-plane TEM analysis, and thus it was possible to qualitatively correlate the strain field underneath the indenter with nanocrystallization levels (that is, nanocrystallization is limited to the contact area); this also indicates that the nanocrystallization is induced by indentation, not by sample preparation. Further efforts to develop a precise way (conceivably supported by computational simulations) to quantify critical strain conditions for the nanocrystallization under different indenters are desirable for better understanding of the phenomena.

Acknowledgments

This research was supported by Basic Science Research Program through the National Research Foundation of Korea (NRF) funded by the Ministry of Education, Science and Technology (No. 2010-0025526). Authors would like to thank Dr. H. Bei for providing the BMG rod and Ms. Jong-Min Kim for helping the TEM operation.

References

[1] C.A. Schuch, T.C. Hufnagel, U. Ramamurty, Acta Mater. 55 (2007) 4067–4109.
[2] R. Raghavan, P. Murali, U. Ramamurty, Acta Mater. 57 (2009) 3332–3340.
[3] H. Chen, Y. He, G.J. Shiflet, S.J. Poon, Nature 367 (1994) 541–543.
[4] W.H. Jiang, M. Atzmon, Scr. Mater. 54 (2006) 333–336.
[5] J.J. Kim, Y. Choi, S. Suresh, A.S. Argon, Science 295 (2002) 654–657.
[6] C.A. Schuh, T.G. Nieh, J. Mater. Res. 19 (2004) 46–57.
[7] M.J. Kramer, D.J. Sordelet, A.F. Bastarows, X. Tan, S.B. Biner, J. Non-Cryst. Solids 351 (2005) 2159–2165.
[8] J. Fornell, E. Rossinyol, S. Surinach, M.D. Baro, W.H. Li, J. Sort, Scr. Mater. 62 (2010) 13–16.
[9] K. Eswar Prasad, N. Chollacoop, U. Ramamurty, Acta Mater. 59 (2011) 4343–4355.
[10] B.-G. Yoo, K.-W. Park, J.-C. Lee, U. Ramamurty, J.-I Jang, J. Mater. Res. 24 (2009) 1405–1416.
[11] J.-I. Jang, M.J. Lance, S. Wen, T.Y. Tsui, G.M. Pharr, Acta Mater. 53 (2005) 1759–1770.
[12] J.-I. Jang, B.-G. Yoo, J.-Y. Kim, Appl. Phys. Lett. 90 (2007) 211906.
[13] B.-G. Yoo, J.-Y. Kim, J.-I. Jang, Mater. Trans. 48 (2007) 1765–1769.
[14] B.B. Sun, Y.B. Yang, J. Wen, H. Yang, M.L. Sui, J.Q. Wang, E. Ma, Scr. Mater. 53 (2005) 805–809.
[15] Z. Altounian, E. Batalla, J.O. Strom-Olsen, J.L. Walter, J. Appl. Phys. 61 (1987) 149–155.